FRONTIERS OF PHYSICS

RESEARCH ARTICLE
Volume 19 / Issue 2 / 21201 / 2024

Local quantum Fisher information and quantum correlation in the mixed-spin Heisenberg *XXZ* chain

Peng-Fei Wei[1,*], Qi Luo[1,*], Huang-Qiu-Chen Wang[1], Shao-Jie Xiong[2], Bo Liu[3,†], Zhe Sun[1,4,‡]

1 School of Physics, Hangzhou Normal University, Hangzhou 310036, China
2 Zhejiang Institute of Modern Physics and School of Physics, Zhejiang University, Hangzhou 310027, China
3 School of Information and Electrical Engineering, Hangzhou City University, Hangzhou 310015, China
4 Zhejiang Provincial Key Laboratory of Urban Wetlands and Regional Change, Hangzhou 311121, China
*These two authors contributed equally to this work.
Corresponding authors. E-mail: †liuboheqingbo@126.com, ‡sunzhe@hznu.edu.cn
Received April 6, 2023; accepted August 8, 2023

ABSTRACT

We study the local quantum Fisher information (LQFI) in the mixed-spin Heisenberg *XXZ* chain. Both the maximal and minimal LQFI are studied and the former is essential to determine the accuracy of the quantum parameter estimation, the latter can be well used to characterize the discord-type quantum correlations. We investigate the effects of the temperature and the anisotropy parameter on the maximal LQFI and thus on the accuracy of the parameter estimation. Then we make use of the minimal LQFI to study the discord-type correlations of different site pairs. Different dimensions of the subsystems cause different values of the minimal LQFI which reflects the asymmetry of the discord-type correlation. In addition, the site pairs at different positions of the spin chains have different minimal LQFI, which reveals the influence of the surrounding spins on the bipartite quantum correlation. Our results show that the LQFI obtained through a simple calculation process provides a convenient way to investigate the discord-type correlation in high-dimensional systems.

Keywords local quantum Fisher information, quantum correlation, mixed-spin Heisenberg *XXZ* chain

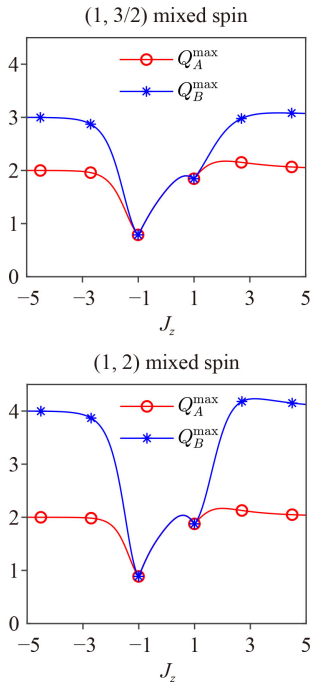

1 Introduction

Quantum metrology, as a rapidly developing field of quantum technology, can achieve higher precision and sensitivity measurements than classical proposals. According to the quantum Cramér–Rao theorem, the quantum Fisher information (QFI) lies at the heart of quantum metrology, which provides the lower bound on the variance of an unbiased estimator. In recent years, various proposals of quantum metrology and quantum parameter estimation have been successfully implemented in different physical systems [1–12]. In addition to quantum metrology, the QFI has been well applied in other important issues, such as entanglement witness [13–15], quantum phase transition detection [16, 17], and non-

Higher Education Press

https://doi.org/10.1007/s11467-023-1336-9

Markovianity measure [18].

Recently, the concept of local quantum Fisher information (LQFI) is proposed in Ref. [19], which defines the QFI of a bipartite system while the parameter to be estimated is introduced via a local unitary evolution. The minimum LQFI is found to be able to naturally quantify the guaranteed sensitivity that a bipartite probe state allows in an interferometric configuration. It can also be used to quantify the discord-type quantum correlation and provide an experimental demonstration of the usefulness of discord in sensing applications. In Ref. [20], the minimum LQFI is used to characterize the non-Markovianity of open systems in local decoherence channels. In Ref. [21], LQFI is used to describe the quantum-correlation dynamics of two non-interacting qubits driven by a single classical field pattern with random phases. In Ref. [22], LQFI is used to analyze the influence of cavity dissipation and spontaneous emission on two-magnon dynamics for different magnon–magnon and photon–magnon couplings. Then, the LQFI was investigated in the anisotropic XY Heisenberg spin chain [23], where the LQFI was found to depend on the temperature and the coupling parameter. The LQFI was also studied in the Heisenberg XYZ chain with Dzyaloshinskii–Moriya interaction [24–28], where the authors found the Dzyaloshinskii–Moriya interaction can enhance the value of LQFI. However, most of the aforementioned works mainly focused on the two-site spin-1/2 Heisenberg chains. There is currently a lack of research on the situations of high-dimensional systems, e.g., the spin length is larger than 1/2 and the total site number is larger than two. In this work we for the first time consider the LQFI in the $(1/2, S)$ mixed-spin chain, then the LQFI corresponding to the spin-S subsystem will present different behaviors from the spin-1/2 subsystem, and which can reveal the asymmetry of the discord-type correlation. Moreover, by increasing the total site number of the spin chain, the LQFI of different site pairs can be considered, which will exhibit the influence of the surrounding sites on the LQFI.

This paper is organized as follows. In Section 2, we introduce the definition of the LQFI and the calculation method of the maximal and minimal LQFI. In Section 3, we investigate the LQFI in the two-site $(1/2, S)$ mixed-spin XXZ Heisenberg chain and analytically calculate both of the maximal and minimal LQFI. In Section 4, we numerically study the relationship between the maximal LQFI of the subsystem and the temperature T as well as the anisotropy parameter J_z. In Section 5, we compare the quantum discord with the minimal and maximal LQFI and further consider the minimal LQFI of different site pairs. The $(1/2, S)$ mixed-spin cases with $S = 1, 3/2, 2$ are considered and the total size of the spin chain is enlarged to 6 sites. In Section 6, we add the second and third nearest-neighbor coupling and discuss the influence on the minimum LQFI. Conclusions are given in Section 7.

2 Local quantum Fisher information

The parameterized state ρ_θ can be expressed by $\rho_\theta = U_\theta \rho U_\theta^\dagger$, where the initial state $\rho = \sum_{i=1}^{D} \lambda_i |\psi_i\rangle\langle\psi_i|$ does not hold the parameter θ, and U_θ is the unitary operator to lead into the parameter θ. Here, D is the dimension of the support set of ρ, λ_i and $|\psi_i\rangle$ are the i-th eigenvalue of ρ and the corresponding eigenstate, respectively. Then QFI is expressed as [29, 30]

$$\mathcal{F} = \sum_{i=1}^{D} 4\lambda_i \langle\psi_i \left|H^2\right| \psi_i\rangle - \sum_{i,j=1}^{D} \frac{8\lambda_i\lambda_j}{\lambda_i+\lambda_j} \left|\langle\psi_i \left|H\right| \psi_j\rangle\right|^2 . \tag{1}$$

Here, $H := \mathrm{i}\,(\partial_\theta U_\theta^\dagger) U_\theta$ is a Hermitian operator.

In this paper, we consider a bipartite state ρ_{AB} in the Hilbert space $\mathcal{H}_A^{N_A} \otimes \mathcal{H}_B^{N_B}$, where N_A and N_B denote the dimensions of the subsystems A and B, respectively. Assuming the dynamic evolution of the subsystem A is $U_A = \mathrm{e}^{\mathrm{i}\theta \tilde{H}_A}$ with the local Hamiltonian $\tilde{H}_A = H_A \otimes I_B$, the LQFI of the subsystem A is written as

$$\mathcal{F}(\rho_{AB}, H_A) = 4\mathrm{Tr}(\rho \tilde{H}_A^2) - \sum_{i,j=1}^{D} \frac{8\lambda_i\lambda_j}{\lambda_i+\lambda_j} \left|\langle\psi_i \left|\tilde{H}_A\right| \psi_j\rangle\right|^2 . \tag{2}$$

For a $2 \times N_B$-dimensional bipartite state, the local Hamiltonian is chosen as $H_A = \boldsymbol{x} \cdot \boldsymbol{s}$, where $\boldsymbol{s} = (\sigma_x, \sigma_y, \sigma_z)/2$ with the Pauli matrices $\{\sigma_{x,y,z}\}$, and $\boldsymbol{x} = (x_1, x_2, x_3)$ with $|\boldsymbol{x}| = 1$. Then, LQFI of subsystem A can be rewritten as

$$\begin{aligned}\mathcal{F}(\rho_{AB}, H_A) =& 1 - \sum_{m,n=1}^{3} \sum_{i,j=1}^{D} \frac{2\lambda_i\lambda_j}{\lambda_i+\lambda_j} \langle\psi_i |\sigma_m \otimes I| \psi_j\rangle \\ & \times \langle\psi_j|\sigma_n \otimes I|\psi_i\rangle x_m x_n .\end{aligned} \tag{3}$$

Here, $\lambda_{i(j)}$ are the eigenvalues of density matrix ρ_{AB} with the corresponding eigenvectors $|\psi_{i(j)}\rangle$.

The LQFI of the subsystem A is rewritten as

$$\mathcal{F}(\rho_{AB}, H_A) = \boldsymbol{x}^{\mathrm{T}} \mathcal{W}^A \boldsymbol{x}. \tag{4}$$

Here, the matrix $\mathcal{W}^A$ is a real symmetric matrix, whose elements are

$$\mathcal{W}^A_{mn} = \delta_{mn} - \sum_{i,j=1}^{D} \frac{2\lambda_i\lambda_j}{\lambda_i+\lambda_j} \langle\psi_i|\sigma_m \otimes I|\psi_j\rangle\langle\psi_j|\sigma_n \otimes I|\psi_i\rangle, \tag{5}$$

where $\delta_{mn} = 1$ (for $m = n$) and $\delta_{mn} = 0$ (for $m \neq n$). We use $\mu_{\max}$ and $\mu_{\min}$ to represent the maximum and minimal eigenvalues of $\mathcal{W}^A$, respectively. Thus, we can define the maximal and the minimal LQFI of the subsystem A as

$$\mathcal{Q}_A^{\max} = \max_{H_A} \mathcal{F} = \mu_{\max}, \quad \mathcal{Q}_A^{\min} = \min_{H_A} \mathcal{F} = \mu_{\min}. \tag{6}$$

Let us consider the subsystem B. The unitary evolution is $U_B = \mathrm{e}^{\mathrm{i}\theta \tilde{H}_B}$ with the local Hamiltonian $\tilde{H}_B = I_A \otimes H_B$. The local Hamiltonian is $H_B = \boldsymbol{y} \cdot \boldsymbol{S}$, where $\boldsymbol{S}$ is the spin operator with the spin length $S > 1/2$ and also let $|\boldsymbol{y}| = 1$. Similarly, the LQFI of the subsystem B is

$$\mathcal{F}(\rho_{AB}, H_B) = \boldsymbol{y}^{\mathrm{T}} \mathcal{W}^B \boldsymbol{y}. \tag{7}$$

Here, $\mathcal{W}^B$ is also a real symmetric matrix with the elements as

$$\begin{aligned} \mathcal{W}^B_{mn} =& \sum_{i=1}^{D} 2\lambda_i \langle \psi_i | I \otimes (S_m S_n + S_n S_m) | \psi_i \rangle \\ & - \sum_{i,j=1}^{D} \frac{8\lambda_i \lambda_j}{\lambda_i + \lambda_j} \langle \psi_i | I \otimes S_m | \psi_j \rangle \langle \psi_j | I \otimes S_n | \psi_i \rangle. \end{aligned} \tag{8}$$

Similarly, the maximal and the minimal LQFI of the subsystem B (i.e., $\mathcal{Q}_B^{\max}$ and $\mathcal{Q}_B^{\min}$) can be obtained by the maximal and minimal eigenvalues of the matrix $\mathcal{W}^B$.

3 LQFI in Heisenberg model

The LQFI in the Heisenberg spin model has been widely studied [23–28]. In this paper, we consider the $(1/2, S)$ mixed-spin Heisenberg XXZ chain with only the nearest-neighbor interaction under the open boundary condition. The system consists of two kinds of spins with different spin lengths alternating on a chain. Its Hamiltonian components are

$$\begin{aligned} H_\alpha &= \sum_{i=1}^{n/2} \left(s_i^\alpha S_i^\alpha + S_i^\alpha s_{i+1}^\alpha \right), \ (\alpha = x, y, z) \\ H &= H_x + H_y + J_z H_z, \end{aligned} \tag{9}$$

where the spin length of the spins $s = 1/2$ and $S > 1/2$. J_z is the anisotropy parameter and n is the number of sites (n is chosen as even numbers in this work). The open boundary condition is considered, i.e., we set $s^\alpha_{n/2+1} = 0$.

Let us first focus on the two-site case, i.e., $n = 2$, and the spin-1/2 and spin-S are denoted by the subsystems A and B, respectively. Then the density matrix of this system in thermal equilibrium can be described by the Gibbs state at the temperature T, i.e., $\rho(T) = \exp(-\beta H)/Z$ with the partition function $Z \equiv \mathrm{Tr}[\exp(-\beta H)]$, and $\beta = 1/(k_{\mathrm{B}} T)$ (here the Boltzmann constant is set as $k_{\mathrm{B}} = 1$). When we choose the eigenstates of the operator $s_z + S_z$ to be the basis, i.e., $\{|-1/2, -1\rangle, |-1/2, 0\rangle, |-1/2, 1\rangle, |1/2, -1\rangle, |1/2, 0\rangle, |1/2, 1\rangle\}$, the eigenvalues of the Hamiltonian (9) can be easily obtained as $E_1 = E_2 = J_z/2$, $E_3 = E_4 = -(J_z + \sqrt{J_z^2 + 8})/4$, and $E_5 = E_6 = -(J_z - \sqrt{J_z^2 + 8})/4$. Based on the definition in Eqs. (5) and (8), one can find that the off-diagonal matrix elements of $\mathcal{W}^A$ and $\mathcal{W}^B$ for the subsystems A and B are zero and the diagonal matrix elements are obtained as

$$\begin{aligned} \mathcal{W}^A_{11(22)} =& 1 - \frac{8}{Z} \left[\frac{ab}{(a+b)(2E_5^2+1)} + \frac{ac}{(a+c)(2E_3^2+1)} \right. \\ & \left. + \frac{2bcE_3^2}{(b+c)(2E_3^2+1)^2} + \frac{bE_5^2 + cE_3^2}{2(2E_3^2+1)(2E_5^2+1)} \right], \\ \mathcal{W}^B_{11(22)} =& \frac{4}{Z} \left[a + \frac{4b(b-a)E_5^2}{(a+b)(2E_5^2+1)} + \frac{4c(c-a)E_3^2}{(a+c)(2E_3^2+1)} \right. \\ & \left. - \frac{4bc(2E_3^2-1)^2}{(b+c)(2E_3^2+1)^2} + \frac{2(E_3^2 b + E_5^2 c) - 3(b+c)}{(2E_3^2+1)(2E_5^2+1)} \right], \\ \mathcal{W}^{A(B)}_{33} =& \frac{8(b-c)^2}{Z(b+c)(2E_3^2+1)(2E_5^2+1)}. \end{aligned} \tag{10}$$

Here, $a = \exp(-\beta E_1)$, $b = \exp(-\beta E_3)$, and $c = \exp(-\beta E_5)$. Thus, the maximal and the minimal LQFI for the subsystems A and B can be obtained from the diagonal elements of $\mathcal{W}^A$ and $\mathcal{W}^B$. Then one can find that the diagonal elements are $\mathcal{W}^A_{33} = \mathcal{W}^B_{33}$.

Limiting temperature cases. Now, let us discuss the limiting temperature cases:

(i) When the temperature $T \to 0$, we should take different regions of J_z into account. For $J_z > -1$, the diagonal elements are

$$\begin{aligned} \mathcal{W}^A_{11(22)} &= \frac{4E_3^2 \left(E_3^2 + 1\right)}{\left(2E_3^2 + 1\right)^2}, \\ \mathcal{W}^B_{11(22)} &= \frac{8E_3^4 - 4E_3^2 + 4}{(2E_3^2 + 1)^2}, \\ \mathcal{W}^{A(B)}_{33} &= \frac{8E_3^2}{(2E_3^2 + 1)^2}. \end{aligned} \tag{11}$$

Thus, in this case, we have $\mathcal{Q}_A^{\max} = \mathcal{W}^A_{33}$ and $\mathcal{Q}_A^{\min} = \mathcal{W}^A_{11}$ for $J_z \in (-1, 1]$, while $\mathcal{Q}_A^{\max} = \mathcal{W}^A_{11}$ and $\mathcal{Q}_A^{\min} = \mathcal{W}^A_{33}$ for $J_z \in (1, \infty)$. For the subsystem B, we have $\mathcal{Q}_B^{\max} = \mathcal{W}^B_{11}$ and $\mathcal{Q}_B^{\min} = \mathcal{W}^B_{33}$ for $J_z \in (-1, 0] \cup [1, \infty)$, while $\mathcal{Q}_B^{\max} = \mathcal{W}^B_{33}$ and $\mathcal{Q}_B^{\min} = \mathcal{W}^B_{11}$ for $J_z \in (0, 1)$. Since the diagonal elements $\mathcal{W}^A_{33} = \mathcal{W}^B_{33}$, the behavior of $\mathcal{Q}_A^{\max}$ ($\mathcal{Q}_A^{\min}$) can be consistent with that of $\mathcal{Q}_B^{\max}$ ($\mathcal{Q}_B^{\min}$) in some regions of J_z, e.g., we have $\mathcal{Q}_A^{\max} = \mathcal{Q}_B^{\max}$ for $J_z \in [0, 1]$ and $\mathcal{Q}_A^{\min} = \mathcal{Q}_B^{\min}$ for $J_z \in [1, \infty)$.

For $J_z < -1$, we have

$$\begin{aligned} \mathcal{W}^A_{11(22)} &= 1, \\ \mathcal{W}^B_{11(22)} &= 2, \\ \mathcal{W}^{A(B)}_{33} &= 0, \end{aligned} \tag{12}$$

thus, $\mathcal{Q}_A^{\max} = 1$, $\mathcal{Q}_A^{\min} = 0$, $\mathcal{Q}_B^{\max} = 2$, and $\mathcal{Q}_B^{\min} = 0$.

When we consider the special point $J_z = -1$, all the diagonal elements of $\mathcal{W}^A$ and $\mathcal{W}^B$ equal to $4/9$, which means $\mathcal{Q}_A^{\max} = \mathcal{Q}_B^{\max} = \mathcal{Q}_A^{\min} = \mathcal{Q}_B^{\min} = 4/9$. At another special

point $J_z = 1$, there is $\mathcal{Q}_A^{\max} = \mathcal{Q}_B^{\max} = \mathcal{Q}_A^{\min} = \mathcal{Q}_B^{\min} = 8/9$. The special results can be attributed to the high degeneracy of the eigenstates at $J_z = \pm 1$ where the anisotropy disappears.

(ii) For the limit temperature $T \to \infty$, whatever the value of J_z is, all the diagonal elements of $\mathcal{W}^A$ and $\mathcal{W}^B$ equal to zero, and thus $\mathcal{Q}_A^{\max} = \mathcal{Q}_A^{\min} = \mathcal{Q}_B^{\max} = \mathcal{Q}_B^{\min} = 0$. It implies that the thermal fluctuation will eventually destroy all the quantum Fisher information and quantum correlations.

4 Relationship between the maximum LQFI and the parameters

Based on the method of Eqs. (5)–(8), we can obtain the maximal LQFI of the subsystems A and B ($\mathcal{Q}_{A,B}^{\max}$) even for high-dimensional operators. In this part, we will discuss the relationship between $\mathcal{Q}_{A,B}^{\max}$ and the temperature T as well as the anisotropy parameter J_z. The maximal QFI is essential to determine the precision of quantum parameter estimations.

4.1 Maximal LQFI versus different temperatures

We numerically study the effect of the temperature on the maximal LQFI. In Fig. 1, the two-site case ($n = 2$) in Eq. (9) is considered and the anisotropy parameter is set as $J_z = 3, 2, 1/2$. The spin length is $s = 1/2$ for the subsystem A and $S = 1$, 3/2, and 2 for the subsystem B, respectively. The maximum LQFI for the subsystems A and B ($\mathcal{Q}_A^{\max}$ and $\mathcal{Q}_B^{\max}$) are defined by Eq. (6). As shown in Fig. 1, with the increase of temperature T, both $\mathcal{Q}_A^{\max}$ (the red line with circles) and $\mathcal{Q}_B^{\max}$ (the blue line with stars) gradually decrease to zero.

In addition, our results clearly show that the subsystems A and B with different dimensions hold different LQFI. We find that at the low temperatures, when $|J_z| > 1$, the value of $\mathcal{Q}_B^{\max}$ is larger than that of $\mathcal{Q}_A^{\max}$ and the difference between them increases as the spin length S increases. However, when $|J_z| \leq 1$, the rule may be broken, e.g., when $J_z = 1/2$ the difference between $\mathcal{Q}_B^{\max}$ and $\mathcal{Q}_A^{\max}$ in the case of $S = 2$ [see Fig. 1(k)] is smaller than that of $S = 3/2$ [see Fig. 1(h)] at the low temperatures. When the temperature rises high enough, the difference between the $\mathcal{Q}_A^{\max}$ and $\mathcal{Q}_B^{\max}$ will disappears gradually for all the values of J_z. While, larger J_z and larger spin length S may lead to a higher threshold temperature at which $\mathcal{Q}_A^{\max}$ and $\mathcal{Q}_B^{\max}$ become consistent with each other.

4.2 Maximal LQFI versus different values of the parameter J_z

We take into account the effect of the anisotropy parameters J_z on the maximal LQFI for the temperature $T = 0.5$. In Figs. 2(a)–(c), the spin length $s = 1/2$ for the subsystem A and $S = 1$, 3/2, 2 for the subsystem B. Due to the different dimensions of the subsystems A and B, the values of $\mathcal{Q}_A^{\max}$ and $\mathcal{Q}_B^{\max}$ are different. When $|J_z| > 1$, $\mathcal{Q}_B^{\max}$ (the blue line with stars) is bigger than $\mathcal{Q}_A^{\max}$ (the red line with circles). Moreover, both of the $\mathcal{Q}_A^{\max}$ and $\mathcal{Q}_B^{\max}$ increase with the increase of the absolute value $|J_z|$. That means the maximal quantum Fisher information, i.e., the accuracy of the parameter estimation, can be improved by increasing the absolute value of J_z. In the region $|J_z| \leq 1$, the dependence of $\mathcal{Q}_{A,B}^{\max}$ on the absolute value $|J_z|$ may be different, e.g., larger $|J_z|$ can lead to smaller values of $\mathcal{Q}_{A,B}^{\max}$.

In the range of $J_z \in [-1, 1]$, $\mathcal{Q}_A^{\max}$ equals to $\mathcal{Q}_B^{\max}$. This may be due to the special energy level structure in this region. We show the energy levels versus parameter J_z in Figs. 2(d)–(f), where one can find the energy levels intersect at the point of $J_z = \pm 1$, i.e., the high degeneracy of the eigenstates occurs at the points. In the region $J_z \in [-1, 1]$, all the energy levels are close to each other. At finite temperatures, the eigenstates become to be mixed together with the weights corresponding to their eigenenergies, and the degenerate states hold equal weights. The special structure of the mixed state for $J_z \in [-1, 1]$ may be one of the reasons why the difference

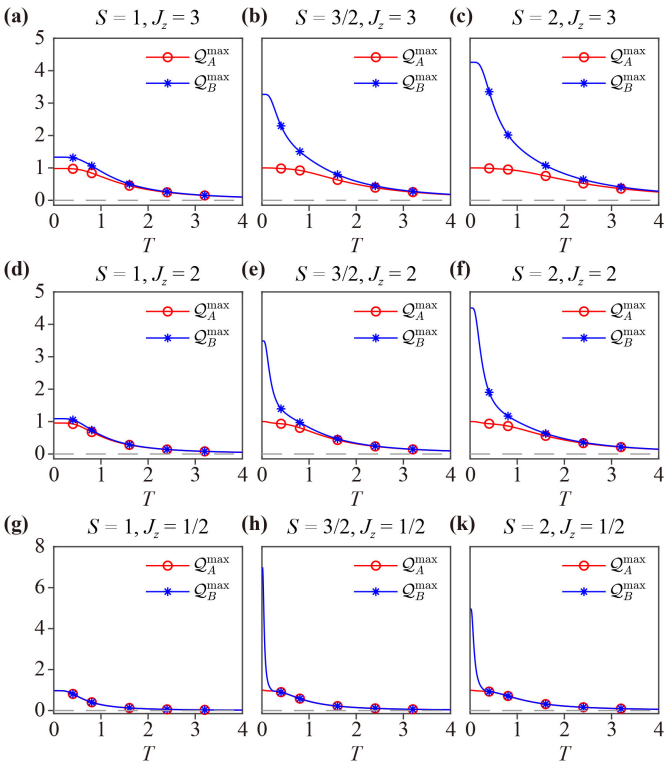

Fig. 1 For the two-site case of the Hamiltonian in Eq. (9), $\mathcal{Q}_A^{\max}$ and $\mathcal{Q}_B^{\max}$ vary with temperature T. We choose the spin length $s = 1/2$ for the subsystem A and $S = 1$ **(a, d, g)**, $S = 3/2$ **(b, e, h)**, and $S = 2$ **(c, f, k)** for the subsystem B. The anisotropy parameters is $J_z = 3$ **(a)**–**(c)**, $J_z = 2$ **(d)**–**(f)**, and $J_z = 1/2$ **(g)**–**(k)**.

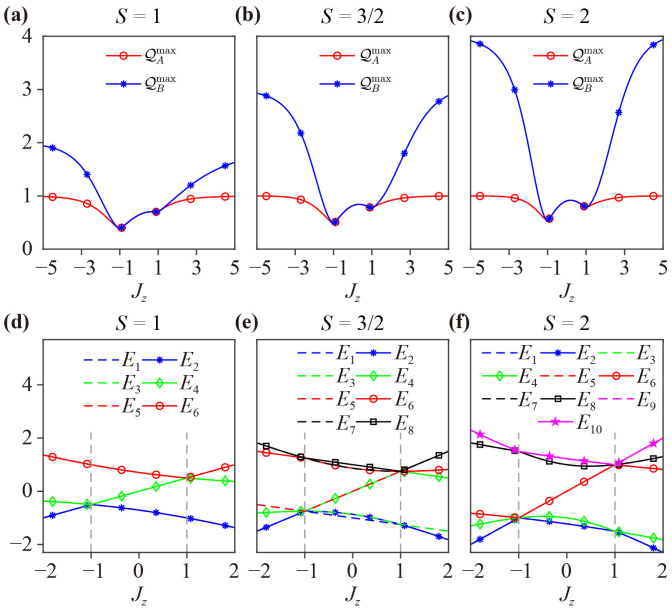

Fig. 2 For the two-site case of the Hamiltonian in Eq. (9) with $T = 0.5$, in subfigures **(a–c)** $\mathcal{Q}_{A,B}^{\max}$ and in subfigures **(d–f)** the corresponding eigen energy levels vary with J_z. The spin length is $s = 1/2$ for the subsystem A and $S = 1$ **(a, d)**, $S = 3/2$ **(b, e)**, and $S = 2$ **(c, f)** for subsystem B.

between $\mathcal{Q}_A^{\max}$ and $\mathcal{Q}_B^{\max}$ disappears. We find that it requires a threshold temperature. For the case of two-site $(1/2, 1)$ mixed spin chain, we numerically find that when the temperature reaches about $T_{\text{th}} \approx 0.178$, $\mathcal{Q}_A^{\max}$ and $\mathcal{Q}_B^{\max}$ become consistent in the region $J_z \in [-1, 1]$. When the temperature is lower than that, the behaviors of the $\mathcal{Q}_A$ and $\mathcal{Q}_B$ tend to follow the analytical results shown in the case of $T \to 0$ in Eqs. (11) and (12). For the two sites $(1/2, 3/2)$, the threshold temperature is about $T_{\text{th}} \approx 0.317$, and for the two sites $(1/2, 2)$, the threshold temperature becomes $T_{\text{th}} \approx 0.429$. We show more numerical results of different mixed-spin cases for different temperatures in Appendix A. In addition, we also increase the spin length of the subsystem A to $s = 1$, and investigate the change rule of J_z. Compared with the result of Fig. 2, it can be found that the increase of spin length of the subsystem A will also bring some different behavior rules, see Appendix A for details.

5 LQFI and quantum correlation

5.1 LQFI and quantum discord

For a bipartite state, quantum discord is defined as [31]

$$D_Q^{A\to B}(\rho_{AB}) \equiv \min_{\Pi_i^A} \left[\mathcal{I}(\rho_{AB}) - \mathcal{J}(\rho_{AB})_{\Pi_i^A}\right]. \tag{13}$$

Here, $\mathcal{I}(\rho_{AB}) = S(\rho_A) + S(\rho_B) - S(\rho_{AB})$ represents the mutual information between the subsystems A and B

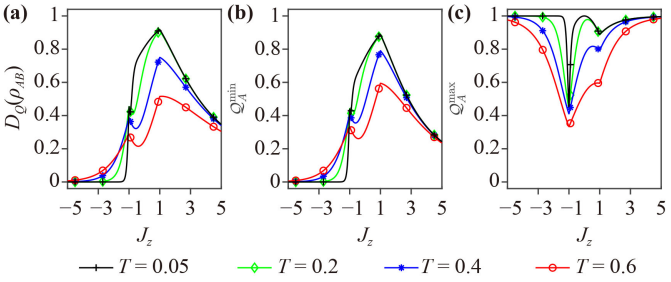

Fig. 3 For the two-site $(1/2, 1)$ mixed-spin chain, $D_Q^{A\to B}$ in **(a)**, $\mathcal{Q}_A^{\min}$ in **(b)**, and $\mathcal{Q}_A^{\max}$ in **(c)** vary with the anisotropy parameter J_z at different temperature $T = 0.05,\ 0.2,\ 0.4,\ 0.6$.

[32]. $S(\rho) \equiv -\text{Tr}(\rho \log_2 \rho)$ is the von Neumann entropy of the density matrix ρ, and $\rho_{A(B)}$ is the reduced density matrix of the subsystem. $\mathcal{J}(\rho_{AB})_{\Pi_i^A} = S(\rho_B) - S(\rho_B|\Pi_i^A)$ is the amount of information gained about the subsystem B by measuring the subsystem A. $\{\Pi_i^A\}$ are the measurement operators corresponding to the von Neumann measurement on the subsystem A. $S(\rho_B|\Pi_i^A)$ is the conditional entropy after the measurement performed on the subsystem A. Generally, D_Q is asymmetric for the different subsystems A and B, which is therefore defined by $D_Q^{A\to B}$ or $D_Q^{B\to A}$ for distinction [32, 33]. Quantum discord can be used to describe the quantum correlation even when the quantum entanglement disappears. Especially, in dissipative systems, the quantum discord is more robust than quantum entanglement [34, 35]. The quantum discord has been well applied in many systems to describe the quantum correlations [36–42]. For the general states, the analytical and numerical calculation of quantum discord is complicated because of the optimization process over all the local generalized measurements. Therefore, it is only possible to obtain the analytical expressions of quantum discord for certain classes of states.

It has been proved that the minimal LQFI satisfies all the established criteria to be a measure of discord-type quantum correlations [19]. Thus, in this work, we employ the minimal LQFI to characterize the bipartite correlation in the mixed-spin chain. We first compare the behaviors of the quantum discord $D_Q^{A\to B}$, the minimal LQFI ($\mathcal{Q}_A^{\min}$), and the maximal LQFI ($\mathcal{Q}_A^{\max}$) versus different parameters J_z. Different temperatures are also considered.

In Fig. 3, for the two-site $(1/2, 1)$ mixed-spin chain with spin-1/2 for the subsystem A and spin-1 for the subsystem B, we numerically calculate the quantum discord $D_Q^{A\to B}$ versus different J_z, and the temperature is set to $T = 0.05$, 0.2, 0.4, and 0.6 [see Fig. 3(a)]. Then, the results of $\mathcal{Q}_A^{\min}$ are shown in Fig. 3(b). One can find that $D_Q^{A\to B}$ and $\mathcal{Q}_A^{\min}$ follow a basically consistent behavior. They both reach the peak value at $J_z = 1$ and reach the secondary peak at $J_z = -1$.

For comparison, we numerically calculate the maximal

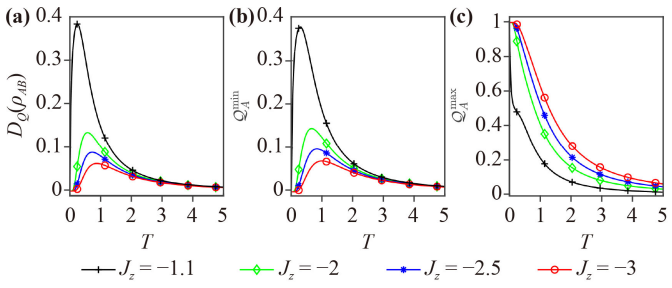

Fig. 4 For the two-site $(1/2, 1)$ mixed-spin chain, $D_Q^{A\to B}$ in **(a)**, $\mathcal{Q}_A^{\min}$ in **(b)**, and $\mathcal{Q}_A^{\max}$ in **(c)** vary with different temperatures for different parameters J_z.

LQFI ($\mathcal{Q}_A^{\max}$) in Fig. 3(c). Different from $\mathcal{Q}_A^{\min}$ ($D_Q^{A\to B}$), $\mathcal{Q}_A^{\max}$ reaches the minimum values at $J_z = \pm 1$. In the regions of $|J_z| > 1$, one can find that the increasing (decreasing) $\mathcal{Q}_A^{\max}$ corresponds to the decreasing (increasing) $\mathcal{Q}_A^{\min}$ and $D_Q^{A\to B}$. However, the situation is different for the region of $|J_z| \leq 1$, where the behaviors of $\mathcal{Q}_A^{\min}$ and $D_Q^{A\to B}$ become nonmonotonic, and the three quantities $\mathcal{Q}_A^{\min}$, $D_Q^{A\to B}$, and $\mathcal{Q}_A^{\max}$ can increase together for some values of J_z.

We can understand the phenomena that when $J_z < -1$, the system tends to the ferromagnetic structure, i.e., the ground state can be treated as a direct product state of states with consistent spin orientations at all sites. Obviously, there is no quantum correlation, thus $D_Q^{A\to B}$ and $\mathcal{Q}_A^{\min}$ have zero values. When the temperature increases, different spin orientations will occur. This leads to a certain quantum correlation in the system state. As the temperature continues to rise, more excited states are mixed in. This makes the system tend towards a completely mixed state, thereby disrupting the quantum correlation. On the other hand, in the case of antiferromagnetism such as $J_z > 1$, the ground state tends to be the superposition state or mixed state consisting of the components with the opposite-oriented spins alternately on the chain. Therefore, the ground state initially has quantum correlations, and the increasing temperature will weaken the quantum correlation.

The maximal LQFI ($\mathcal{Q}_A^{\max}$) is different from the minimal LQFI $\mathcal{Q}_A^{\min}$, which is related to the accuracy of parameter estimation. As the temperature increases, the thermal fluctuation will destroy the quantum resource and thus reduce the accuracy of the quantum parameter estimation. Therefore, in all the considered regions of J_z, increasing temperature always has a negative effect on $\mathcal{Q}_A^{\min}$.

In order to show the effect of the temperature more clearly, we calculate $D_Q^{A\to B}$, $\mathcal{Q}_A^{\min}$, and $\mathcal{Q}_A^{\max}$ versus temperature in Fig. 4 and find that in the region of $J_z < -1$, the dependence of $\mathcal{Q}_A^{\min}$ and $D_Q^{A\to B}$ on temperature is nonmonotonic. $\mathcal{Q}_A^{\min}$ and $D_Q^{A\to B}$ first increase with the temperature from zero values to their maximum values, then decrease gradually. However, the influence of the temperature T on $\mathcal{Q}_A^{\max}$ is obviously different from that on $\mathcal{Q}_A^{\min}$ and $D_Q^{A\to B}$. Raising the temperature always lowers the value of $\mathcal{Q}_A^{\max}$ regardless of the value of J_z.

5.2 The minimal LQFI of different site pairs

Since the minimal QFI ($\mathcal{Q}_{A,B}^{\min}$) can be a measure of discord-type quantum correlations, we make use of $\mathcal{Q}_{A,B}^{\min}$ to study the bipartite correlations of a pair of sites on the spin chain. Several effects will be considered, such as the subsystem dimension, the total number of the spin sites, the position of the site pairs, and the distance between the two sites.

First, we take into account the impact of the total number of the spin sites on the minimal LQFI. We choose the site number as $n = 2, 4, 6$, and two types of spin with $s = 1/2$ (corresponding to the subsystem A) and $S = 1$ (corresponding to the subsystem B) alternately distribute on the spin chain. The site pair considered by us consists of the 1-st and 2-nd sites (denoted by "sites 1 & 2"). Then, we show $\mathcal{Q}_{A,B}^{\min}$ of the sites 1 & 2 varying with J_z at temperature $T = 0.5$ in Figs. 5(a) and (b). In most cases within the range of J_z, the $\mathcal{Q}_A^{\min}$ of $n = 4$ (the blue line with stars) and $n = 6$ (the red line with circles) are below the case of $n = 2$ (the green line with rhombus). There is only a slight difference between the two curves of $n = 4$ and $n = 6$. We also check the 8-site chain and find the similar phenomena with those of $n = 4$ and $n = 6$. The spin chain in this work is considered under the open boundary condition, and the sites far from the chosen sites have a weak correlation with them. Thus, increasing the total site number to 6 and 8 only introduces a slight influence on the minimal LQFI of the sites 1 & 2.

Comparing $\mathcal{Q}_A^{\min}$ and $\mathcal{Q}_B^{\min}$ in subfigures (a) and (b), one may find some different behaviors between them. For example, in the region of $J_z \in [-1, 0]$, the values of $\mathcal{Q}_B^{\min}$ of $n = 4$ and $n = 6$ can be slightly larger than those of $n = 2$. The difference between $\mathcal{Q}_A^{\min}$ and $\mathcal{Q}_B^{\min}$ also reflects the asymmetry of the discord-type correlations. We show the results of the two-site $(1/2, 3/2)$ and $(1/2, 2)$ mixed-spin chain in Appendix B, where more obvious differences between $\mathcal{Q}_A^{\min}$ and $\mathcal{Q}_B^{\min}$ can be found.

Second, we focus on the different positions of the spin pairs. Three nearest-neighbour pairs, i.e., 1 & 2, 3 & 4, and 5 & 6, are considered. Then, we calculate $\mathcal{Q}_{A,B}^{\min}$ versus J_z at temperature $T = 0.5$ and show the results in Figs. 5(c) and (d). We find that different positions of the site pairs provide different values of $\mathcal{Q}_{A,B}^{\min}$, which reflects the different influences of the surrounding sites when the spin pair under consideration is placed at the edges or in the center of the spin chain. Different values and behaviors between $\mathcal{Q}_A^{\min}$ and $\mathcal{Q}_B^{\min}$ can also be found.

In addition, we consider the effect of the distance between the two sites. In Figs. 5(e) and (f), the $\mathcal{Q}_{A,B}^{\min}$ of the spin pairs consist of the sites 1 & 2 (green line with rhombus), the sites 1 & 4 (blue line with stars), and the sites 1 & 6 (red line with circles). Obviously, $\mathcal{Q}_{A,B}^{\min}$

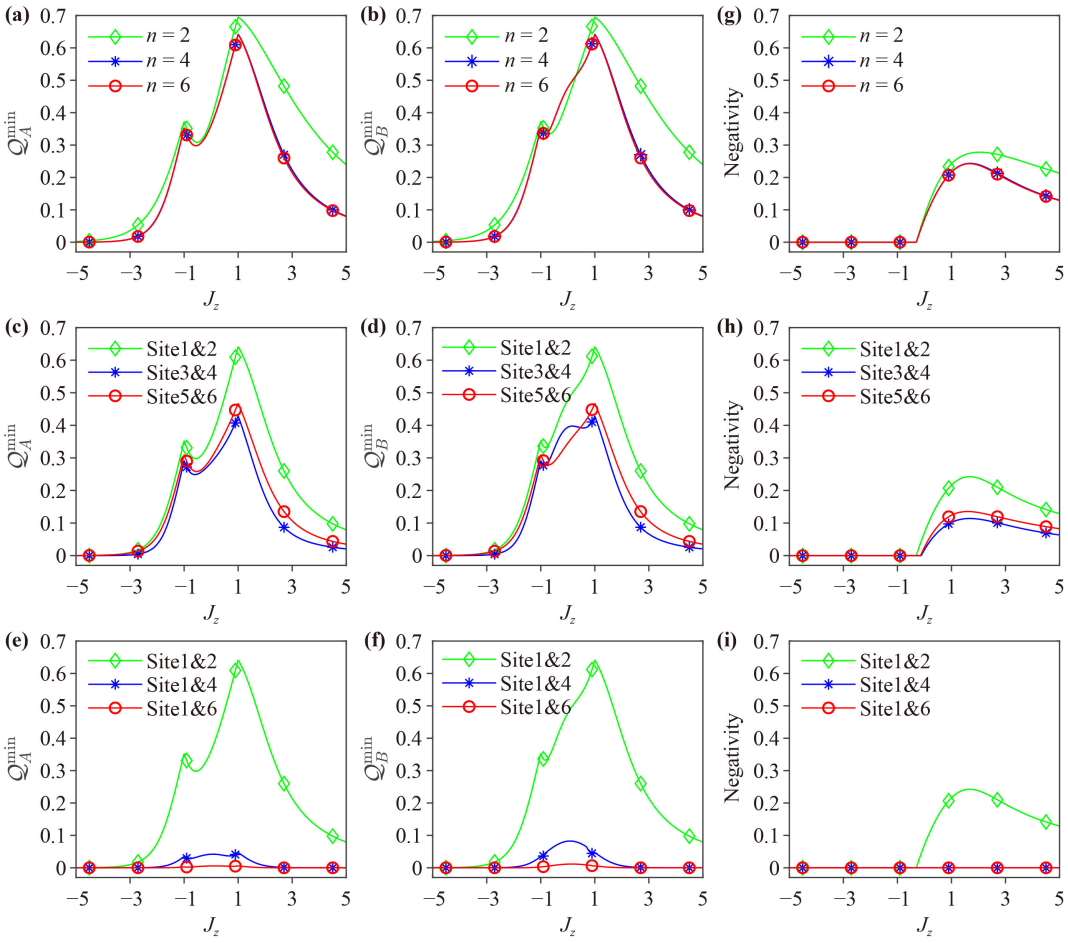

Fig. 5 The subgraphs **(a, b)** show the $\mathcal{Q}_{A,B}^{\min}$ of the site 1 & 2 varies with J_z for different total site number $n = 2$, 4, 6. In **(c, d)**, the 6-site spin chain is considered and the results show the $\mathcal{Q}_{A,B}^{\min}$ of the sites 1 & 2, 3 & 4, and 5 & 6 varying with J_z. In **(e, f)** the 6-site spin chain is considered and the results show the $\mathcal{Q}_{A,B}^{\min}$ of the sites 1 & 2, 1 & 4, and 1 & 6 varies with J_z. The subgraphs **(g–i)** show the results of the negativity which is used to describe the entanglement of the site pairs. Here, we choose spin-1/2 for the subsystem A and spin-1 for the subsystem B at temperature $T = 0.5$.

decrease with the increase of the distance between the sites of the subsystems A and B. In this type of spin chain, the bipartite correlations cannot exist between two sites at a long distance.

For comparison, the entanglement (measured by the negativity [43, 44]) is discussed and the results are shown in Figs. 5(g)–(i). One can find that in the region of $J_z \in [-3, -1]$, $\mathcal{Q}_{A,B}^{\min}$ becomes evidently larger than zero, while the negativity keeps a zero value. In addition, entanglement can be easily suppressed or destroyed. When we increase the distance between the two sites under consideration, the entanglement (measured by the negativity) disappears for the site pair 1 & 4 in the whole region of J_z [see Fig. 5(i)]. By contrast, the discord-type correlation (measured by $\mathcal{Q}_{A,B}^{\min}$) presents nonzero values in an approximate region of $J_z \in (-2, 2)$. In the case of two-site $(1/2, 3/2)$ and $(1/2, 2)$ mixed-spin chain shown in Appendix B, one can see the phenomena more clearly.

6 LQFI in multiple nearest-neighbor coupling Heisenberg model

In this section, we have discussions on the impact of the second and third nearest-neighbor coupling. Then, the corresponding Hamiltonian can be expressed as

$$H_\alpha = \sum_{i=1}^{n/2} \left[J_1 \left(s_i^\alpha S_i^\alpha + S_i^\alpha s_{i+1}^\alpha \right) + J_2 \left(s_i^\alpha s_{i+1}^\alpha + S_i^\alpha S_{i+1}^\alpha \right) + J_3 \left(s_i^\alpha S_{i+1}^\alpha + S_i^\alpha s_{i+2}^\alpha \right) \right], \ (\alpha = x, y, z) \tag{14}$$

where J_1, J_2, and J_3 are the first, second, and third nearest-neighbor interaction intensities, respectively. For simplicity, we set $J_k = 1$, $(k = 1, 2, 3)$. The open boundary condition is considered, i.e., we set $s_{n/2+1}^\alpha = 0$, $S_{n/2+1}^\alpha = 0$, $s_{n/2+2}^\alpha = 0$.

Then, for the Hamiltonian with the second and third nearest-neighbor coupling, we calculated the $\mathcal{Q}_{A,B}^{\min}$ of the

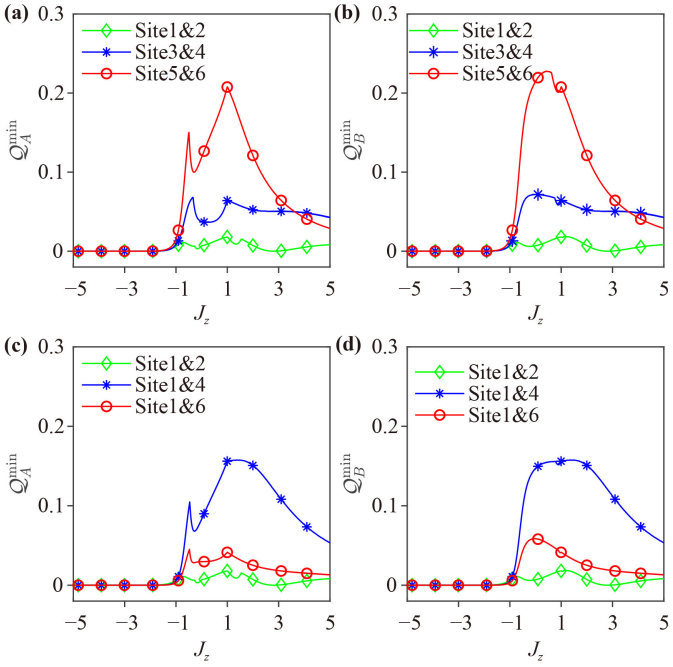

Fig. 6 The subgraphs **(a, b)** show the $\mathcal{Q}_{A,B}^{\min}$ of the sites 1 & 2, 3 & 4, and 5 & 6 varying with J_z. The subgraphs **(c, d)** show the $\mathcal{Q}_{A,B}^{\min}$ of the sites 1 & 2, 1 & 4, and 1 & 6 varying with J_z. Here, we choose spin-1/2 for the subsystem A and spin-1 for the subsystem B at temperature $T = 0.5$.

nearest-neighbor sites, i.e., 1 & 2, 3 & 4, and 5 & 6, varying with J_z [see Figs. 6(a) and (b)]. Compared to Figs. 5(c, d), quite different results are shown in Figs. 6(a) and (b). Especially, the curve of the $\mathcal{Q}_{A,B}^{\min}$ between 1 & 2 sites (green line with rhombus) becomes the lowest one, while the $\mathcal{Q}_{A,B}^{\min}$ between 5 & 6 sites become the highest one.

We also considered the $\mathcal{Q}_{A,B}^{\min}$ of the 1 & 2, 1 & 4, and 1 & 6 sites varying with J_z [see Figs. 6(c) and (d)]. Compared to Figs. 5(e) and (f), the $\mathcal{Q}_{A,B}^{\min}$ of the 1 & 2 sites (green line with rhombus) in Figs. 6(c) and (d) significantly decreases, while the $\mathcal{Q}_{A,B}^{\min}$ of the 1 & 6 sites (red line with circles) and the $\mathcal{Q}_{A,B}^{\min}$ of the 1 & 4 sites (blue line with stars) increase. Thus, the second and third nearest-neighbor coupling present remarkable effect on the minimal LQFI (i.e., the discord-type correlation), i.e., they enhance the $\mathcal{Q}_{A,B}^{\min}$ of the high-order-neighbor sites and suppress the $\mathcal{Q}_{A,B}^{\min}$ of the nearest-neighbor sites.

7 Conclusion

We investigate the LQFI and bipartite quantum correlations in the mixed-spin Heisenberg XXZ chain. Both the maximal LQFI ($\mathcal{Q}_{A,B}^{\max}$) and the minimal LQFI ($\mathcal{Q}_{A,B}^{\min}$) are considered in this work. The former determines the accuracy of the parameter estimation and the latter can measure the discord-type quantum correlation.

We find that the increasing temperature will suppress the maximal LQFI ($\mathcal{Q}_{A,B}^{\max}$) to zero values. The dependence of $\mathcal{Q}_{A,B}^{\max}$ on the anisotropy parameter J_z is complicated. In the region $|J_z| > 1$, the larger $|J_z|$ leads to the larger $\mathcal{Q}_{A,B}^{\max}$. While, in the region $|J_z| \leq 1$, the dependence of $\mathcal{Q}_{A,B}^{\max}$ on the absolute value $|J_z|$ may be different, e.g., larger $|J_z|$ can lead to smaller values of $\mathcal{Q}_{A,B}^{\max}$. Different dimensions of the subsystems can lead to different values of $\mathcal{Q}_{A,B}^{\max}$.

Then we make use of the minimal LQFI ($\mathcal{Q}_{A,B}^{\min}$) to characterize the discord-type correlation. Different dimensional subsystems can provide different values of $\mathcal{Q}_{A,B}^{\min}$, which reflects the asymmetry of the discord-type correlation. In most regions of the anisotropy parameter J_z, the higher dimensional subsystem can provide larger $\mathcal{Q}_{A,B}^{\min}$. We find that the temperature can affect $\mathcal{Q}_{A,B}^{\min}$ either positively or negatively, which depends on the value of the J_z. When the spin chain with more sites (e.g., $n = 6$) is considered, we find that the site pair at different positions of the chain holds different values of $\mathcal{Q}_{A,B}^{\min}$. The $\mathcal{Q}_{A,B}^{\min}$ of the nearest-neighbour sites is larger than that of the site pairs consisting next-nearest-neighbour or farther apart sites. Our results show that the minimal LQFI can well describe the discord-type correlation, especially in the case of the high dimensions. Compared with the original definition of quantum discord, the calculation of the minimal LQFI is much simpler since there is no need for the optimization process over all the local generalized measurements.

Declarations The authors declare that they have no competing interests and there are no conflicts.

Acknowledgements The work was supported by the National Natural Science Foundation of China (NSFC) under Grant No. 12175052 and the Postdoctoral Science Foundation of China (No. 2022M722794).

Appendix A

For the two-site $(1/2, S)$ mixed-spin Heisenberg chain, $\mathcal{Q}_A^{\max}$ and $\mathcal{Q}_B^{\max}$ vary with the parameter J_z at different temperatures and for different S in Fig. A1. For $S = 1$ in the subfigures Figs. A1(a)–(c), $\mathcal{Q}_A^{\max}$ is smaller than $\mathcal{Q}_B^{\max}$ in most range of J_z. When the temperature is higher than $T_{\text{th}} \approx 0.178$, $\mathcal{Q}_A^{\max}$ and $\mathcal{Q}_B^{\max}$ are consistent with each other in the region of $J_z \in [-1, 1]$. For $S = 3/2$ in the subfigures Figs. A1(d)–(f), $\mathcal{Q}_A^{\max}$ equals to $\mathcal{Q}_B^{\max}$ in the region of $J_z \in [-1, 1]$ at the threshold temperature about $T_{\text{th}} \approx 0.317$. For $S = 2$ in the subfigures Figs. A1(g)–(i), the threshold temperature is about $T_{\text{th}} \approx 0.429$.

We also increase the spin length of the subsystem A to $s = 1$, and calculate two mixed spin cases $(1, 3/2)$ and $(1, 2)$ [see Fig. A2]. Comparing the results in Fig. A2 and

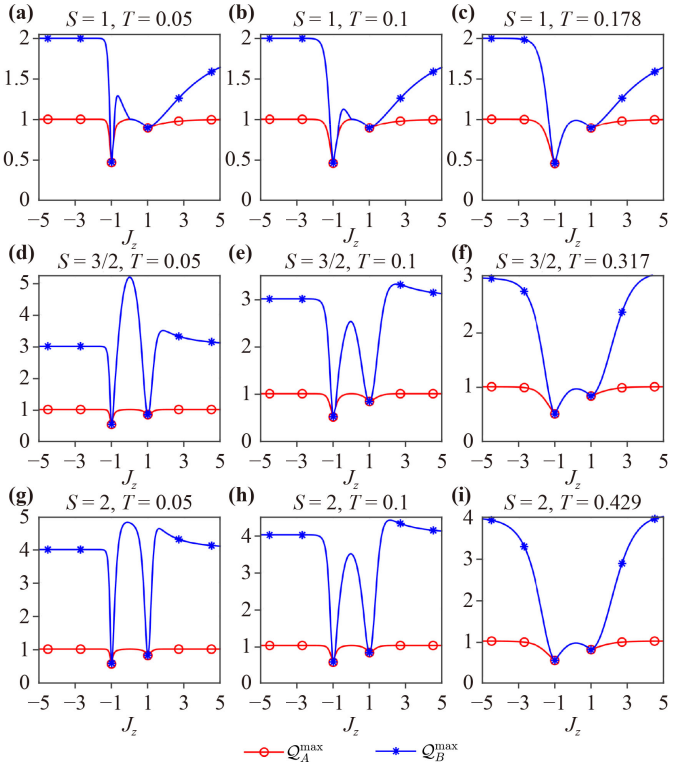

Fig. A1 In the two-site $(1/2, S)$ mixed-spin chain, $\mathcal{Q}_{A,B}^{\max}$ versus the parameter J_z at different temperatures. The subgraphs **(a, b, c)** correspond to the case of $S = 1$, the subgraphs **(d, e, f)** correspond to the case of $S = 3/2$, and the subgraphs **(g, h, i)** correspond to the case of $S = 2$.

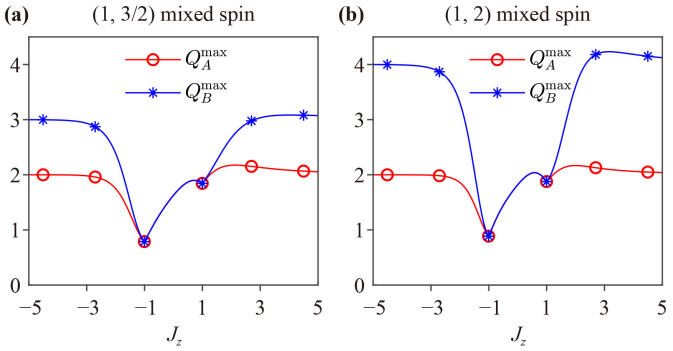

Fig. A2 For the two-site case of the Hamiltonian in Eq. (9) with $T = 0.5$, $\mathcal{Q}_A^{\max}$ and $\mathcal{Q}_B^{\max}$ vary with J_z.The spin length is $s = 1$ for the subsystem A and $S = 3/2$ **(a)** and $S = 2$ **(b)** for the subsystem B.

Fig. 2, we find that the values of $\mathcal{Q}_A^{\max}$ (the red line with circles) significantly increases when we increase the spin length of the subsystem A to $s = 1$, but the value of $\mathcal{Q}_B^{\max}$ (the blue line with stars) does not increase significantly. We also find some new phenomena in Fig. A2 that when $J_z < -2$, both of the $\mathcal{Q}_A^{\max}$ and $\mathcal{Q}_B^{\max}$ increase to their steady values more quickly than that in the $(1/2, S)$ case (in Fig. 2). In addition, when $J_z > 2$, the values of $\mathcal{Q}_{A,B}^{\max}$ present a slightly decrease with the increased value of J_z

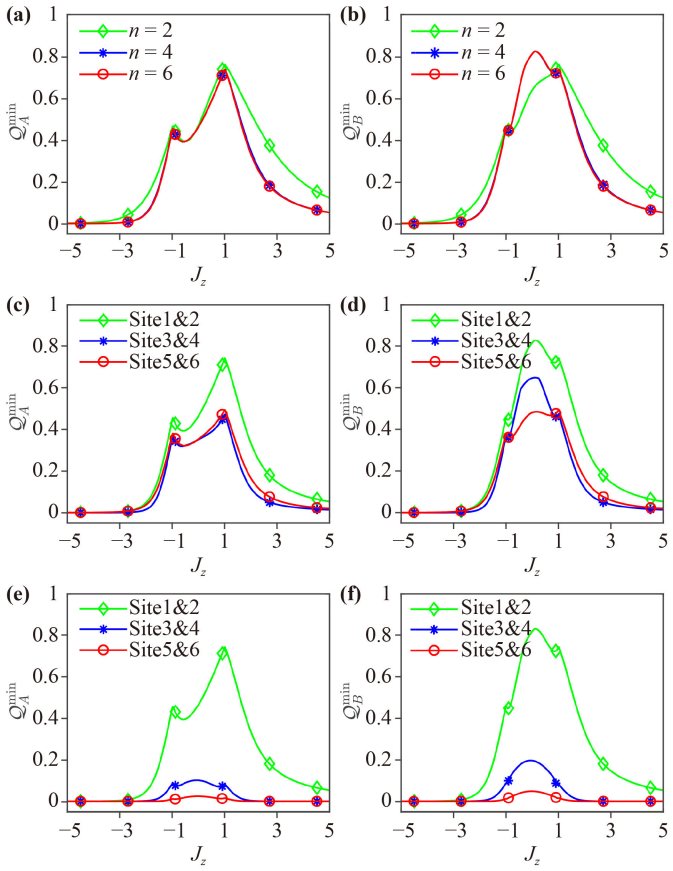

Fig. B1 $\mathcal{Q}_A^{\min}$ **(a, c, e)** and $\mathcal{Q}_B^{\min}$ **(b, d, f)** versus the parameter J_z at the temperature $T = 0.5$ in the two-site $(1/2, 3/2)$ mixed-spin chain.

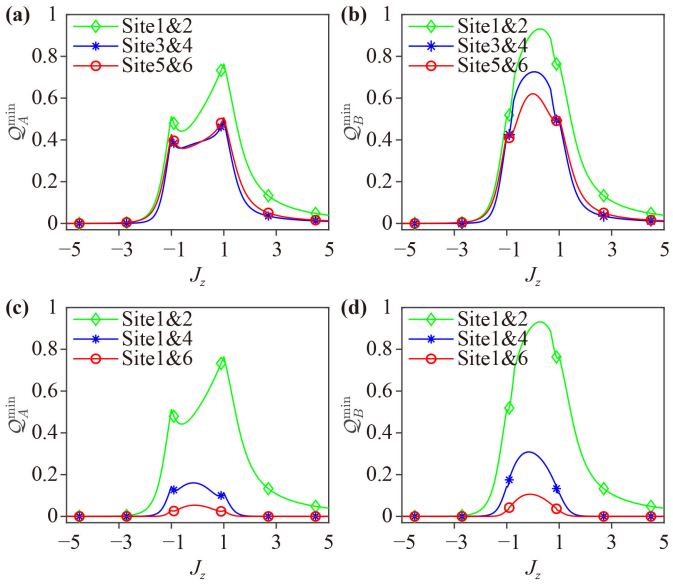

Fig. B2 $\mathcal{Q}_A^{\min}$ **(a, c)** and $\mathcal{Q}_B^{\min}$ **(b, d)** versus the parameter J_z at the temperature $T = 0.5$ in the two-site $(1/2, 2)$ mixed-spin chain.

which cannot be found in the $(1/2, S)$ case in Fig. 2 during the considered region of J_z.

Appendix B

For the two-site $(1/2, 3/2)$ mixed-spin Heisenberg chain, $\mathcal{Q}_A^{\max}$ and $\mathcal{Q}_B^{\max}$ vary with the parameter J_z in Fig. B1. The difference between $\mathcal{Q}_A^{\min}$ and $\mathcal{Q}_B^{\min}$ in Fig. B1 is greater than that in Fig. 5.

The variation of $\mathcal{Q}_A^{\min}$ and $\mathcal{Q}_B^{\min}$ with parameters J_z at the temperature $T = 0.5$ in the two-site $(1/2, 2)$ mixed-spin chain has been shown in Fig. B2. We find more obvious differences between $\mathcal{Q}_A^{\min}$ and $\mathcal{Q}_B^{\min}$ when the spin length S increases to 2.

References

1. V. Giovannetti, S. Lloyd, and L. Maccone, Quantum-enhanced measurements: Beating the standard quantum limit, *Science* 306(5700), 1330 (2004)
2. D. Braun, G. Adesso, F. Benatti, R. Floreanini, U. Marzolino, M. W. Mitchell, and S. Pirandola, Quantum-enhanced measurements without entanglement, *Rev. Mod. Phys.* 90(3), 035006 (2018)
3. L. Pezzè, A. Smerzi, M. K. Oberthaler, R. Schmied, and P. Treutlein, Quantum metrology with nonclassical states of atomic ensembles, *Rev. Mod. Phys.* 90(3), 035005 (2018)
4. J. P. Dowling and K. P. Seshadreesan, Quantum optical technologies for metrology, sensing, and imaging, *J. Lightwave Technol.* 33(12), 2359 (2015)
5. J. Liu, M. Zhang, H. Chen, L. Wang, and H. Yuan, Optimal scheme for quantum metrology, *Adv. Quantum Technol.* 5(1), 2100080 (2022)
6. R. Demkowicz-Dobrzański and L. Maccone, Using entanglement against noise in quantum metrology, *Phys. Rev. Lett.* 113(25), 250801 (2014)
7. L. Pezzé and A. Smerzi, Ultrasensitive two-mode interferometry with single-mode number squeezing, *Phys. Rev. Lett.* 110(16), 163604 (2013)
8. R. Schnabel, N. Mavalvala, D. E. McClelland, and P. K. Lam, Quantum metrology for gravitational wave astronomy, *Nat. Commun.* 1(1), 121 (2010)
9. S. D. Huver, C. F. Wildfeuer, and J. P. Dowling, Entangled Fock states for robust quantum optical metrology, imaging, and sensing, *Phys. Rev. A* 78(6), 063828 (2008)
10. M. Ahmadi, D. E. Bruschi, C. Sab'ın, G. Adesso, and I. Fuentes, Relativistic quantum metrology: Exploiting relativity to improve quantum measurement technologies, *Sci. Rep.* 4(1), 4996 (2014)
11. Z. Sun, J. Ma, X. M. Lu, and X. G. Wang, Fisher information in a quantum-critical environment, *Phys. Rev. A* 82(2), 022306 (2010)
12. M. Zhang, H. M. Yu, H. D. Yuan, X. G. Wang, R. Demkowicz-Dobrzański, and J. Liu, QuanEstimation: An open-source toolkit for quantum parameter estimation, *Phys. Rev. Res.* 4(4), 043057 (2022)
13. S. J. Gu, Fidelity approach to quantum phase transitions, *Int. J. Mod. Phys. B* 24(23), 4371 (2010)
14. T. L. Wang, L. N. Wu, W. Yang, G. R. Jin, N. Lambert, and F. Nori, Quantum Fisher information as a signature of the superradiant quantum phase transition, *New J. Phys.* 16(6), 063039 (2014)
15. U. Marzolino and T. Prosen, Fisher information approach to non-equilibrium phase transitions in a quantum *XXZ* spin chain with boundary noise, *Phys. Rev. B* 96(10), 104402 (2017)
16. P. Hyllus, W. Laskowski, R. Krischek, C. Schwemmer, W. Wieczorek, H. Weinfurter, L. Pezzé, and A. Smerzi, Fisher information and multiparticle entanglement, *Phys. Rev. A* 85(2), 022321 (2012)
17. G. Tóth, Multipartite entanglement and high-precision metrology, *Phys. Rev. A* 85(2), 022322 (2012)
18. X. M. Lu, X. Wang, and C. P. Sun, Quantum Fisher information flow and non-Markovian processes of open systems, *Phys. Rev. A* 82(4), 042103 (2010)
19. D. Girolami, A. M. Souza, V. Giovannetti, T. Tufarelli, J. G. Filgueiras, R. S. Sarthour, D. O. Soares-Pinto, I. S. Oliveira, and G. Adesso, Quantum discord determines the interferometric power of quantum states, *Phys. Rev. Lett.* 112(21), 210401 (2014)
20. H. S. Dhar, M. N. Bera, and G. Adesso, Characterizing non-Markovianity via quantum interferometric power, *Phys. Rev. A* 91(3), 032115 (2015)
21. L. P. Chen and Y. N. Guo, Dynamics of local quantum uncertainty and local quantum fisher information for a two-qubit system driven by classical phase noisy laser, *J. Mod. Opt.* 68(4), 217 (2021)
22. A. B. A. Mohamed and H. Eleuch, Dynamics of two magnons coupled to an open microwave cavity: Local quantum Fisher- and local skew-information coherence, *Eur. Phys. J. Plus* 137(7), 853 (2022)
23. A. Slaoui, L. Bakmou, M. Daoud, and R. Ahl Laamara, A comparative study of local quantum Fisher information and local quantum uncertainty in Heisenberg *XY* model, *Phys. Lett. A* 383(19), 2241 (2019)
24. N. Habiballah, Y. Khedif, and M. Daoud, Local quantum uncertainty in *XYZ* Heisenberg spin models with Dzyaloshinski–Moriya interaction, *Eur. Phys. J. D* 72(9), 154 (2018)
25. F. Ozaydin and A. A. Altintas, Parameter estimation with Dzyaloshinski–Moriya interaction under external magnetic fields, *Opt. Quantum Electron.* 52(2), 70 (2020)
26. F. Ozaydin and A. A. Altintas, Quantum metrology: Surpassing the shot-noise limit with Dzyaloshinskii–Moriya interaction, *Sci. Rep.* 5(1), 16360 (2015)
27. S. Haseli, Local quantum Fisher information and local quantum uncertainty in two-qubit Heisenberg *XYZ* chain with Dzyaloshinskii–Moriya interactions, *Laser Phys.* 30(10), 105203 (2020)
28. A. V. Fedorova and M. A. Yurischev, Behavior of quantum discord, local quantum uncertainty, and local quantum Fisher information in two-spin-1/2 Heisenberg chain with DM and KSEA interactions, *Quantum Inform. Process.* 21(3), 92 (2022)
29. J. Liu, X. X. Jing, W. Zhong, and X. G. Wang, Quantum Fisher information for density matrices with arbitrary ranks, *Commum. Theor. Phys.* 61(1), 45 (2014)
30. M. A. Nielsen and I. L. Chuang, Quantum Computation and Quantum Information, Cambridge: Cambridge

University Press, 2000
31. H. Ollivier and W. H. Zurek, Quantum discord: A measure of the quantumness of correlations, *Phys. Rev. Lett.* 88(1), 017901 (2001)
32. B. Groisman, S. Popescu, and A. Winter, Quantum, classical, and total amount of correlations in a quantum state, *Phys. Rev. A* 72(3), 032317 (2005)
33. B. Dakić, V. Vedral, and Č. Brukner, Necessary and sufficient condition for nonzero quantum discord, *Phys. Rev. Lett.* 105(19), 190502 (2010)
34. X. M. Lu, Z. J. Xi, Z. Sun, and X. G. Wang, Geometric measure of quantum discord under decoherence, *Quantum Inf. Comput.* 10(11–12), 0994 (2010)
35. T. Werlang, S. Souza, F. F. Fanchini, and C. J. Villas Boas, Robustness of quantum discord to sudden death, *Phys. Rev. A* 80(2), 024103 (2009)
36. A. Datta, A. Shaji, and C. M. Caves, Quantum discord and the power of one qubit, *Phys. Rev. Lett.* 100(5), 050502 (2008)
37. S. L. Luo and S. S. Fu, Geometric measure of quantum discord, *Phys. Rev. A* 82(3), 034302 (2010)
38. L. Henderson and V. Vedral, Classical, quantum and total correlations, *J. Phys. Math. Gen.* 34(35), 6899 (2001)
39. Y. X. Chen and Z. Yin, Thermal quantum discord in anisotropic Heisenberg *XXZ* model with Dzyaloshinskii–Moriya interaction, *Commum. Theor. Phys.* 54(1), 60 (2010)
40. Q. Chen, C. Zhang, S. Yu, X. X. Yi, and C. H. Oh, Quantum discord of two-qubit *X* states, *Phys. Rev. A* 84(4), 042313 (2011)
41. M. Ali, A. R. P. Rau, and G. Alber, Quantum discord for two-qubit *X* states, *Phys. Rev. A* 81(4), 042105 (2010)
42. S. L. Braunstein and C. M. Caves, Statistical distance and the geometry of quantum states, *Phys. Rev. Lett.* 72(22), 3439 (1994)
43. G. Vidal and R. F. Werner, Computable measure of entanglement, *Phys. Rev. A* 65(3), 032314 (2002)
44. Z. Sun, X. G. Wang, A. Z. Hu, and Y. Q. Li, Entanglement properties in mixed-spin Heisenberg systems, *Physica A* 370(2), 483 (2006)